

# **Search and Rescue Robot (SaRR) Final Design Report**

Presented on December 13th, 2024

**Team:** Gorthrop Numman

**SaRR Name:** Landmine

## **Team Members:**

Calvin Pham

Cameron Farid

Karim Elyoussef

Ryan Gonzales

Alex Liou

Selina Marvit

Soloman Khan-Syed

Michael Hwang

Sean Lee

Aidan Astudillo

## **0. Team Member Breakdown**

Note: Subteam leads in **bold**.

Name	Primary Role	Secondary Role(s)	FDR Contribution
Calvin Pham	Project Lead	Sensors/Programming Manufacturing	Sections 3, 4, 8
Cameron Farid	Project Lead	Manufacturing Frame and Drivetrain	Sections 1, 3, 5
Karim Elyoussef	<b>Wiring</b>	Sensors/Programming Manufacturing	Section 2
Ryan Gonzales	<b>Sensors/Programming</b>	Wiring Manufacturing	Sections 2, 4, 5, 7
Alex Liou	<b>Frame and Drivetrain</b>	Sensors/Programming Manufacturing	Section 5, 6
Selina Marvit	Frame and Drivetrain	Med-Kit Delivery	Section 3, 5
Soloman Khansyed	<b>Aesthetics and Safety</b>	Wiring Manufacturing	Section 4, 8
Michael Hwang	<b>Manufacturing</b>	Aesthetics and Safety	Sections 1, 3
Sean Lee	<b>Med-Kit Delivery</b>	Frame and Drivetrain Manufacturing	Section 1, 6
Aidan Astudillo	Frame and Drivetrain	Med-Kit Delivery Manufacturing	Section 5

## ***1. Executive Summary***

This project addresses the need for autonomous search and rescue robots (SaRRs), which have become especially of interest in the aftermath of the September 11, 2001 rescue effort. The robot presented is capable of autonomously traversing a field of obstacles to deliver medical supplies to a receptacle. The final design uses two pulley-driven treads with external teeth for added grip, allowing for simple yet efficient wall-climbing, along with a system of eight sensors for autonomous navigation. The design also includes a motorized four-bar linkage for robust medkit delivery to the receptacle.

While testing was done via both open (manual) and closed-loop (autonomous) control, the final design functionality is fully autonomous and includes the following tasks: navigation to a ramp using a beacon light at the upslope; navigation over the ramp ( $<15^\circ$ ) and a through a 3-foot wide chute; traversing a 1-foot wall; navigating to a delivery receptacle via beacon light; and deposition of a 1 kg medical kit (manually inserted at the start of the trial) into the receptacle, all within 2 minutes.

Final measures of the robot's specifications include a frame of 30" by 21", a weight of 38.6 lbs, a budget of \$750, and both autonomous and manual operating modes. The maximum continuous current drawn from the motors is 20 Amps, 10 Amps per drivetrain motor. The motor used to deliver the medkit is not included as it only ever draws current while the robot is stationary. Initial design elements, manufacturing processes, improvements and redesigns, and final robot specifications are documented in this report. The final product is a functional robot that successfully demonstrates all autonomous functionality requirements defined above, completing the course in roughly 1 minute and 48 seconds.

## **2. Introduction**

Search and rescue operations are critical when coordinating disaster response, particularly with natural disasters, destructive conflicts, or similar situations. An effective and efficient procedure can be the difference between life and death, especially when evacuation is not an option - for instance, in situations where structures have collapsed, leaving behind significant amounts of debris and hazardous materials.

Human forces, such as first responders, have often acted as the main search and rescue solution with their specialized training and ability to assess the situation. During the events of 9/11, first responders, including a team now known as the 911th TREC, aimed to get survivors out of the buildings before they collapsed [3]. Their realistic training allowed them to effectively and safely conduct search and rescue operations for ten days. In the days afterward, canine forces joined with rescue teams significantly improving the rate at which survivors could be found due to their enhanced senses.

There are some upsides to human and animal search and rescue teams. Human involvement can come with swift adaptability and judgment and also provides the vital aspect of communicating with living victims. It is much easier for humans, compared to machines, to quickly canvas an area and plan the most effective route and rescue plans. Furthermore, humans can train animals, such as canines, whose senses are stronger than ours to allow for a streamlined process of animal-assisted survivor locating and quick human thinking to save the victim. However, such solutions also come with serious downsides and physical risks. Firstly, the field may have tight spaces or steep climbs that are difficult or impossible for humans and animals to safely pass through. There is additionally a general risk of injury due to the nature of the debris, which can be sharp or unstable for grabbing and stepping on.

The mental consequences of manned search-and-rescue missions should also not be ignored, as rescuers involved may leave the situation with depression or trauma. In an article by the U.S. Army, noncommissioned officer Fred Brown, a member of the earlier mentioned 911th TREC, was quoted as saying, ““...we switched into recovery mode only... We just dealt with it. Many of the young soldiers were recovering unrecognizable bodies, often unable to decipher burnt insulation from the flesh”” [3]. Rescuers are placed into high-stress situations that at times may include grave horrors or issues far beyond their teams’ abilities, leaving a significant negative mental impact.

Many times, these downsides may even be fatal. For example, during 9/11, 3,000 people died, but another 1,000 died and roughly 40,000 more were recognized as sick in the years after due to chronic illnesses caused by inhaling smoke or particulates from the debris [8]. Humans and animals who are involved in rescue operations place themselves at risk of toxic exposure carrying prolonged physical impacts in addition to mental impacts.

Thus, robotic solutions may prove to be a viable search and rescue tactic that maintains much of the advantages of human and animal teams, without most of the downsides. With this, Gorthrop Numman proposes the SaRR (Search and Rescue Robot), nicknamed “Landmine”, for such situations. Emphasizing simplicity and maneuverability, “Landmine” is an autonomous vehicle with the desired capabilities of traversing over obstacles, maneuvering through tight pathways, and navigating to pre-positioned light sources. This robot, though not built for extricating victims from a site or clearing pathways through debris, is still useful for search and rescue as it can deliver life-saving supplies to injured survivors who cannot leave their location. It also serves as a proof of concept for more complex, specific situation-oriented designs.

This project was limited to this scope due to the constraints placed upon the group. Namely, on the financial side, the budget allotted for this project was \$750. While various materials, including two brushed motors and scrap stock for machining, were provided in advance for no cost, this budget was enough to require serious thought and planning for each of the few purchases that were made. Given that all ten members of the group were, and currently are, full-time students, several time and labor constraints also came into play. This project lasted three months with a final testing and end date on December 13, 2024.

Research for the design of this project was focused on stair-climbing robots. In a YouTube video, two demonstrations were performed in which a robot with treads on either side both ascended and descended 5 steps of a wide stairway [6]. The robot's main feature was a shape-changing mechanism at one end of the treads, which allowed it to move smoothly from step to step in both directions. The first demonstration showed the robot's performance with no shape-changing, which rocked slightly along each step but still completed its goal; the second demonstration turned this feature on. Since such a changing design may be too complicated given the group's constraints, the decision was made to instead fix the angle of the frontmost pulley in a way similar to the first demonstration. Additionally, it should be noted that research for the sensor packages used code derived from the source for an I2C time-of-flight distance sensor [10].

The design of the med-kit placement mechanism was inspired by the four-bar linkages taught in the MAE322 lecture [7]. This allows the med-kit to be consistently and stably placed, as it follows the same arc trajectory while maintaining the upright position of the med-kit. It also differs from typical methods of previous years because it extends the med-kit a distance away

from the frontmost end of the robot, preventing the robot from touching the basket and potentially adjusting its position.

Videos of past SaRR designs in previous iterations of the MAE322 course were viewed to analyze designs that succeeded and failed. From this, the team decided to emphasize simplicity and generalizability. To be more specific, it was decided to make the robot as simple as possible to navigate the course, to meet time and financial constraints; and generalizable in its autonomous movement such that if variations arose in the course due to human or robot error, it could still complete its mission. There is also an emphasis on modularity, with consistent bolt-hole sizing and spacing throughout the model, allowing new features to be added to the body without having to disassemble and re-machine.

A photo of the final manufactured SaRR design can be found in Figure 2.1, alongside a final CAD rendering in Figure 2.2. Note that the tread system consists of three 3D printed pulley gears, connected by a belt with teeth. The aluminum chassis holds together all of the electrical components in the center of the robot. The light sensors live close to the floor, as the floor reflects the light from the light source placed low on the bucket. The distance sensors live higher up around the top of the gearbox and towards the front pulley so that the robot reacts to the winding walls of the chute and adjusts itself accordingly, to remain centered along the chute. Sensors are discussed in more detail in Section 5.10. The pulley locations have been chosen with the wall dimensions in mind, as mentioned in Section 5.5.

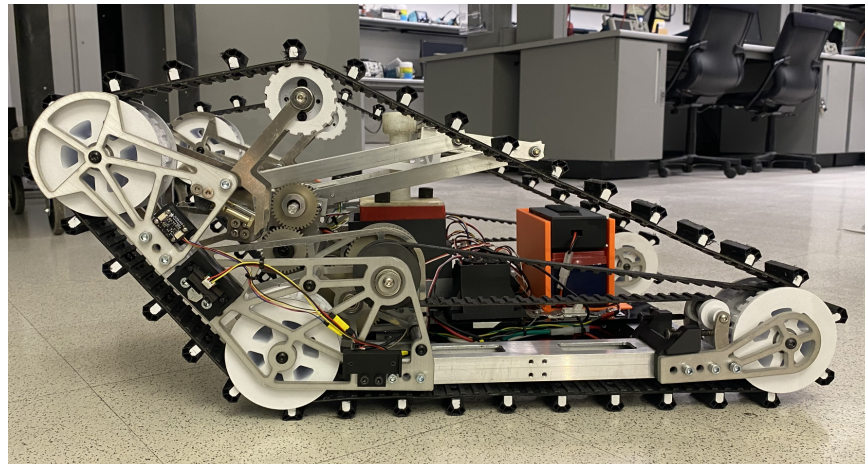


*Figure 2.1: Final manufactured SaRR design*

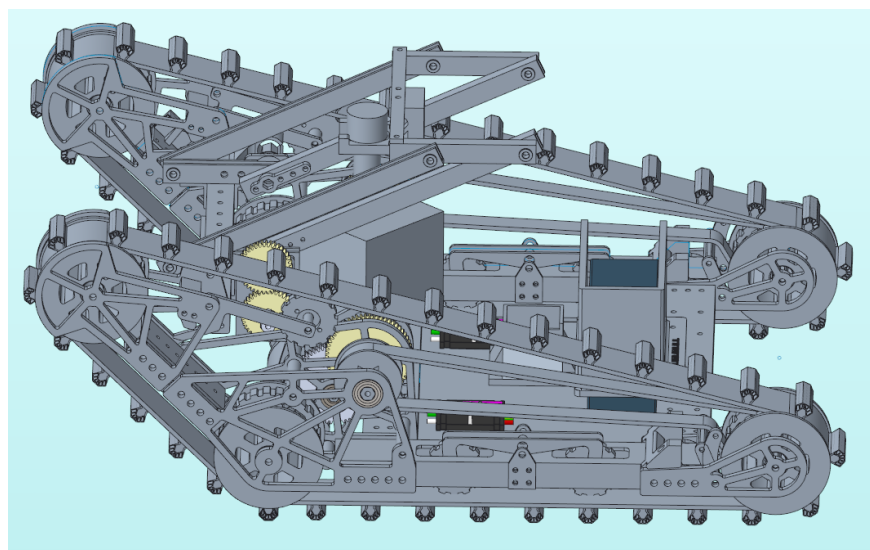


*Figure 2.2: Final Full CAD Render*

### **3. Specifications**

#### **3.1: Weight and Size**

Table 3.1 displays an estimated SaRR weight breakdown, with a total of roughly 40 lbs.

The majority of the weight comes from the mechanical components of the drivetrain and the arm (frame, mounts, etc.). The final weight of the SaRR was measured at 38.6 lbs, indicating that these estimates are reasonable.

Component	Quantity	Weight (lbs)
DT Motors	2	2.8
DT Gearboxes	2	1
Arm Motor	1	2.8
Arm Gearbox	1	1
DT Mechanical	1	15
Arm Mechanical	1	5
Payload	1	2.5
Battery	1	2.75
Electronics	1	3
		<b>Total: ~40 lbs</b>

*Table 3.1: SaRR Weight Estimation Calculations*

The length of the robot is determined by the necessary geometry to traverse the wall, in conjunction with constraints from the chute dimensions. Wall traversal provides a lower bound on length; to successfully climb the steps without tipping backward, the length of the treads effectively “behind” the center of mass while the robot is inclined at 45° must be greater than 8.5” for the treads to maintain contact with both steps (see figure 4.1.5 - 4.1.3). Similarly, in front of the center of mass, the linear distance between the point of contact on the wall and the front of the treads must exceed the 12” height from the wall to the ground—though 12” is an extremely low bound, as it assumes the SaRR would be completely vertical after tipping. Greater distances would decrease the angle of the robot just after tipping, reducing the likelihood of flipping upside down during the wall traversal process. For a more detailed discussion, see Section 5.5.

Increasing the length of the SaRR allows for less required precision in the placement of the CoM, and as such will provide a more robust design. However, increasing the length too much will result in difficulties traversing the chute—particularly, the precision required to navigate the turns—without coming into contact with the sides. Thus, balancing these constraints, the length of the SaRR is 30”.

The width of the SaRR is less critical to the wall traversal. However, it is an important factor in the navigation of the chute—a wider SaRR requires more precision to turn without contacting the sides. The main additions to the width are the motors and motor mounts, which require a minimum of 8.216” per side. Including 2” per side for the frame tube, tread width, and allowances for the med-kit delivery system, the SaRR has a width of 21”.

### **3.2: Speed and Range**

The free speed of the SaRR is, at maximum, 29.4 inches per second. This follows from a 38.6: 1 gear ratio on motors with a free speed RPM of 5330, using 4" wheels (for a more detailed discussion of gearing see Section 5.3). The calculations behind these values can be found in the motors and gearing spreadsheet calculator [here](#) (A.10 of Appendix). The speed is ultimately limited by the current draw of the battery, which we calculate to be near 10A per motor. The range can be estimated by dividing the total battery capacity of the Dakota Lithium 12V 10Ah battery by the total current draw of the motors. Dividing the battery capacity of 10Ah by the total current draw of 20A gives a rough estimate of 30 minutes of runtime, which at a speed of 29.4 inches per second equates to a maximum range over 4,400 feet assuming the SaRR is only driving on flat terrain in a straight line. This calculation does not account for turning, elevation changes, nor the power consumption of the onboard computer, sensors, and med-kit delivery system, making this a sizable overestimate. Regardless, based on this estimate it is highly unlikely that the SaRR will fail to traverse the roughly 80-foot length of the course. This was confirmed in testing, as the SaRR performed multiple, consecutive course runs successfully without needing to recharge.

### **3.3: Traversal Time**

Based on testing, the traversal time is roughly 1 minute and 48 seconds, which is within initial estimates. A robot much faster than this is not practical for autonomous navigation, and a robot much slower would not fulfill its design purpose: In a disaster situation, a traversal time of minutes would allow the SaRR to reach victims in a timely and relevant manner, without leaving them waiting in potentially dangerous situations without medical care for very long. A

theoretical minimum for the time of course traversal can be estimated by dividing the approximate length of the course (~80 feet) by the maximum free speed of the SaRR (29.4 in/s): 32.65 seconds. However, this number is a drastic underestimate due to the slower speed of autonomous navigation and the wall breach which dramatically drops the average running speed. In actuality, the average operating speed of the SaRR is roughly 8.7 in/s.

### **3.4: Operational and Navigational Modes**

During the course traversal, the SaRR functions autonomously through input from both light and distance sensors. Light sensors are used for the ramp and med-kit delivery. The ramp traversal light sensor is used to align the SaRR parallel to the ramp and ensure it is straight when starting the climb. The med-kit light sensor is used to navigate toward the victim after traversing the wall. The distance sensors are used for ramp and chute navigation. The side-mounted Time of Flight sensors ensure the SaRR does not collide with the sides of the chute, while the SHARP sensors ensure that it remains centered on the ramp. Furthermore, the front-mounted distance sensor ensures the SaRR records when it reaches and breaches the wall, activating the program for the next obstacle. Manual open-loop operation was available for testing purposes. More information on sensors and programming is featured in Section 5.10.

## **4. Project Management**

Gorthrop Numman's two team leads - Calvin Pham and Cameron Farid - were tasked with the responsibilities of deliverables and administration. More specifically, the role of the leads was to maintain the timeline of deadlines and milestones; track the budget; and ensure the preliminary and final design report and presentation were prepared for submission.

The main subcomponents were broken into the following departments: Wiring; Sensors and Programming; Frame and Drivetrain; Med-Kit Delivery; Manufacturing, and Aesthetics and Safety. Specific member roles are listed in a chart in Section 0 of this report.

The Wiring department managed all wiring assets related to the robot. With the numerous wires branching from the Teensy board towards the three motors and eight sensors, this team ensured that all connections were stable (in other words, wires would not become disconnected during drop tests or wall traversal) and were tasked with keeping wire runs organized. The Sensors and Programming department was responsible for the autonomous control of the robot. This team made decisions on which sensors to use, designed and printed mounts for each sensor, and developed the program for the robot through extensive testing and tuning.

The Frame and Drivetrain team was responsible for creating the chassis of the robot, as well as its maneuverability through various obstacles. Med-Kit Delivery members designed and developed the mechanism by which the robot delivers the med-kit to the goal. Members of the Manufacturing team were responsible for fabrication and prototyping. This team worked extensively with the Frame and Drivetrain department and the Med-Kit Delivery department on machining the parts they had designed in CAD. Lastly, the Aesthetics and Safety department ensured that all surfaces were safe to touch and that the robot's packaging was clean, cohesive, and eye-catching.

Listed below are the milestone deadlines provided in the course syllabus, with estimates of time committed to each task added at the end of each line.

- Week of October 28th: Demonstrate Autonomous Light Navigation (12 hrs)
- Wednesday, October 30th: Preliminary Design Report Presentation (6 hrs)
- Friday, November 1st: Preliminary Design Report (15 hrs)
- Week of November 4th: Demonstrate Autonomous Ramp and Chute Navigation (20 hrs)
- Week of November 18th: Demonstrate Wall Traversal (20 hrs)
- Week of December 1st: Demonstrate Autonomous Object Placement (30 hrs)
- Friday, December 13th: Final Presentation and Final Design Report (21 hrs)

The company was able to achieve all course-provided milestones within the week of each deadline, except for the autonomous object placement, which was completed shortly after its deadline. Unfortunately, due to complications with the final design, the company was not able to hit the internal “Finalize Mechanical Design” deadline. Initial design testing demanded further iteration for optimization.

The initial risks identified were complications with the manufacturing process and the heavy workload period in November in which three milestones were due. Due to our proactiveness and management, the company was able to avoid the concerns over falling behind in November, as two of the three mentioned milestones - more specifically, the Preliminary Design Report and Wall Traversal - were completed in October. This left ample time for developing the final assembly in November. The only milestone that was nearly missed during this period was Autonomous Ramp and Chute navigation, due to delays in delivering the programming team a fully-maneuverable robot.

Unfortunately, one issue that was not identified until its occurrence was the rise of complications with med-kit deployment. Due to its later occurrence in the timeline, less concern was placed on it which led to a later development and deployment of the system. Combined with unanticipated modification and assembly delays, this led to the company missing the milestone.

As mentioned, additional hours were spent on work outside of the milestones listed above. The general time associated with CAD and manufacturing can be tacked on top of those specific milestones to around the magnitude of 50 hours and 150 hours, respectively, leading to a rough time estimate of 324 hours in total.

The team structure was designed to maximize understanding and communication between members. Every Friday during lab, the plan was to hold a design brief and meeting to ensure all parties were on the same page and address any potential issues. A Discord group chat was created to ensure everyone could easily contact one another in case any concerns arose throughout the week. Lastly, all the work was intended to be stored on the cloud with consistent naming conventions. All CAD files, drawings, .step or .stl files, and Arduino programs were stored in the MAE drive; all other materials, including internal team guidelines, design analyses, and report drafts, were stored in a shared Google Drive.

This initially worked well during the early design phase. However, as weeks passed into the timeline, the design briefs stopped as it was assumed all parties were aware of the design through conversations happening in Discord. As expected, several hours were spent outside of the designated lab times, leading to multiple design changes and fixes throughout the week. This did not pose a major issue, as the involved parties were often generally aware of these changes via communication over Discord. In general, creating the Discord group chat was a successful idea. The same can be said for the team's storage conventions, as this encouraged a more

organized workflow that made it easier to fix issues across departments and share necessary resources for reports and presentations.

The biggest lessons learned pertained to accountability and momentum. There were lulls in the timeline which may have led to delays and the buildup of work towards the end of the semester. These may have been able to be avoided if momentum was kept up. Some possible suggestions for rectifying these issues are to emphasize direct accountability for each person's work; enforce the internal timelines more aggressively so that work can begin earlier and complications can be solved earlier, and be more proactive.

## **5. Detailed Design and Analysis**

### **5.1: Overall Drivetrain Design Considerations**

Multiple drivetrain configurations were under consideration for the SARR, including a tread design, morphing, and/or hybrid stair climbing wheels that change form from a circle to a claw-like shape, large diameter wheels, and other designs. Ultimately, it was decided to build a tread design for simplicity, drive efficiency, and greater confidence in the traversal of the wall due to superior and continuous traction. Additionally, many real-life examples of robots that climb stairs and steep inclines utilize treads for the aforementioned reasons. Thus, the basic premise of the design consists of a continuous tread driven by a pulley or sprocket that produces friction with the ground over a large area and has teeth at uniform intervals to grip the corners and sides of the wall. The front end of the tread will be raised to smoothly grip the first step, raise the robot, and transition the robot to an inclined state. The sizing of the robot, motor, gearbox analysis, and center of mass analysis are reported below.

### **5.2: Mass, Force, and Torque Calculations**

At first, mass analysis was conducted to approximate the mass of the entire robot, as outlined in Table 3.1. For wall traversal, a free-body diagram (Figure 5.2.1) was drawn to determine the forces on the robot assuming a point mass climbing a 45-degree slope. The free body diagram below shows point mass analysis that leads to the following conclusions through trivial mechanics done via spreadsheet calculator [here](#) (A.11 of Appendix).

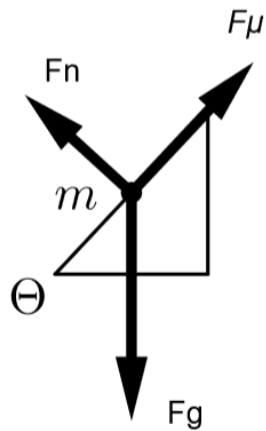


*Figure 5.2.1: Point Mass Slope Analysis*

Using the calculator, it was determined that there would be a requirement for a minimum of 42.4lbf (189N) static holding force  $F_\mu$  given the group's initial 60 lb weight estimate of the robot on a slope of  $\Theta = 45^\circ$ . To enable linear acceleration, a factor of 1.25 is applied to the holding force requirement, leading to a max output force by the treads of 53 lb (236N). This leads to a maximum flat-ground acceleration of  $8.66 \text{ m/s}^2$ , and a slope-climbing acceleration of  $1.73 \text{ m/s}^2$ . A wheel diameter of 4" is chosen for its reasonable radius of curvature for a belt to bend, and so that the robot packages well. Thus, the combined torque requirement on the output shafts of the robot is required to be 106 in-lbf (12 Nm). Given that two separate treads will drive the robot, only half of the force and torque are required per side, requiring 53 in-lbf (5.99 Nm) of torque from each output shaft.

### 5.3: Motor and Gearing Considerations

CIM motors were chosen to supply the required torque for the drivetrain for their high thermal mass, reasonable price, high power, and compatibility with motor controllers. Two options were considered: a one-motor and two-motor per side drivetrain. During analysis, it was

observed that the gearing of the robot is severely current-limited. The battery gives 20 Amps continuously. The motor curve of the CIM shows that the torque from each motor should be around 0.14 Nm for the current to be 10A assuming a two-motor configuration [9]. Thus, the torque must be geared by at least  $6 \text{ Nm} / 0.14 \text{ Nm} = 43:1$ . The original gear ratio chosen was 43.6:1, derived from a 62:9, 62:14, and 20:14 gear ratio through a three-stage gearbox. A custom gearbox and motor design calculator was created using a spreadsheet [here](#) (A.10). This produces an output torque per shaft of 6.1 Nm, greater than the 5.99 Nm requirement set by the team. A two-motor per-side configuration was also considered, and it was observed that there was no benefit to gearing for this configuration. A greater number of motors proved worse since the torque-current curve is linear and there is a free current associated with running the motor at any load.

Ultimately, a mechanical issue with the interference-fit motor pinions on the shafts of the motors led the team to choose a different first stage for the gearbox, changing the gear reduction to 38:1. This performed equivalently to reducing the on-slope multiplicative factor to 1.12 instead of 1.25. Either way, the robot would be able to traverse the wall with a factor greater than 1. Ultimately, the robot mass was much lower than expected, so lowering the torque was never an issue.

#### **5.4: Tread Teeth Design**

To produce sufficient static holding force  $F_\mu$  and prevent slippage, the teeth of the tread must produce sufficient friction in addition to the normal force, as outlined in Figure 5.4.1. To supply this force, the team first observed double-sided timing belts as a less expensive option for tread, since they contained gripping teeth on both sides of the belt. However, after testing some

example belts, the friction and size of these neoprene belts proved insufficient to scale the wall or provide reasonable driving dynamics. Thus, a novel solution was conceived, in which a conventional timing belt would be drilled into using a drill jig and 3D-printed teeth bolted on. These teeth would be interchangeable, modular, and iterative in design to provide the best combination of friction and shape to drive well and climb the wall. The teeth would consist of a PLA core for bolts to secure them, while a low-durometer TPU shell would provide high friction and modular shape.

In the original design, the TPU shell simply wrapped around the PLA core, which was bolted to the tread. However, prototype testing revealed that this was not robust, as the TPU covers would consistently detach from the core when driving, notably during the shock when descending the wall. Thus, the drivetrain team conceived a new design where both the TPU cover and PLA core were bolted to the tread, which proved much more robust in testing. Figure 5.4.2 displays the final tooth CAD profile. The tooth profile uses thin walls to be extremely compliant and grip the floor and wall easily.

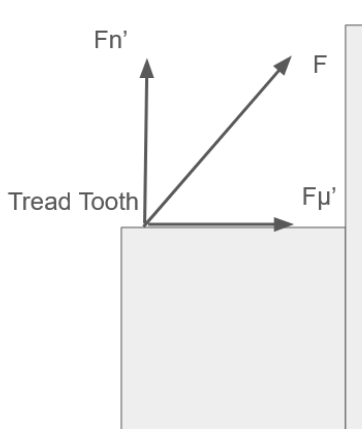


*Figure 5.4.1: Tread Tooth Free Body Diagram*

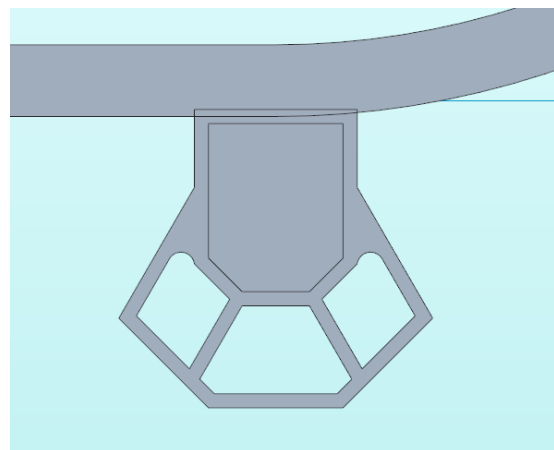


*Figure 5.4.2: Custom Tooth Profile*

## **5.5: Center of Mass Location and Length Constraints**

Figures 5.5.1 - 5.5.3 represent tools to aid the center of mass calculations and dimensional analysis. The flat part of the tread contacting the ground must be long enough to span at least two steps, or around 8.5". When the robot is on the slope in Figure 5.5.1, its center of mass must pass over the highest part of the wall when the treads are still in contact with both steps to produce a moment about the center of mass that will tip the robot over the wall. Thus, the orange line in Figures 5.5.1 and 5.5.2 represents the rearward sloped limit of the center of mass. The center of mass must be in front of this line because if the robot does not tip forward before the tread loses traction with the first step, the robot will begin to pitch up and roll over backward. The forward center of mass is limited by the fact that the robot should remain stable resting parallel to the ground. The center of mass must remain behind the vertical orange line in Figure 5.5.3. Otherwise, when the robot is inclined at a 45-degree angle coming down from the wall, it will flip forward. This yields the range in which our center of mass can lie, which is low and forward relative to the geometry of the robot.

The robot's overall length must be such that when the robot tips over the wall, it does not roll over. Thus, the length of the robot in front of the pivot point (when the center of mass crosses the high point of the wall) must be greater than one foot. If it is exactly one foot, the robot will fall fully vertical. Thus, longer is better, so that, when the nose hits the ground, the pitch is not greater than some threshold. For a 45-degree threshold, this length in front of the pivot is around 17 inches (see triangle in Figure 5.5.4 for trigonometry). Thus, a longer robot allows a greater range of acceptable center of mass options and better tip-forward pitch kinematics. However, the length is limited by the maneuverability of the robot when turning to

traverse the chute. Upon looking at a 2D sketch of how the robot planform fits through 30-degree dogleg turns, it was determined that the length would be 30 inches.

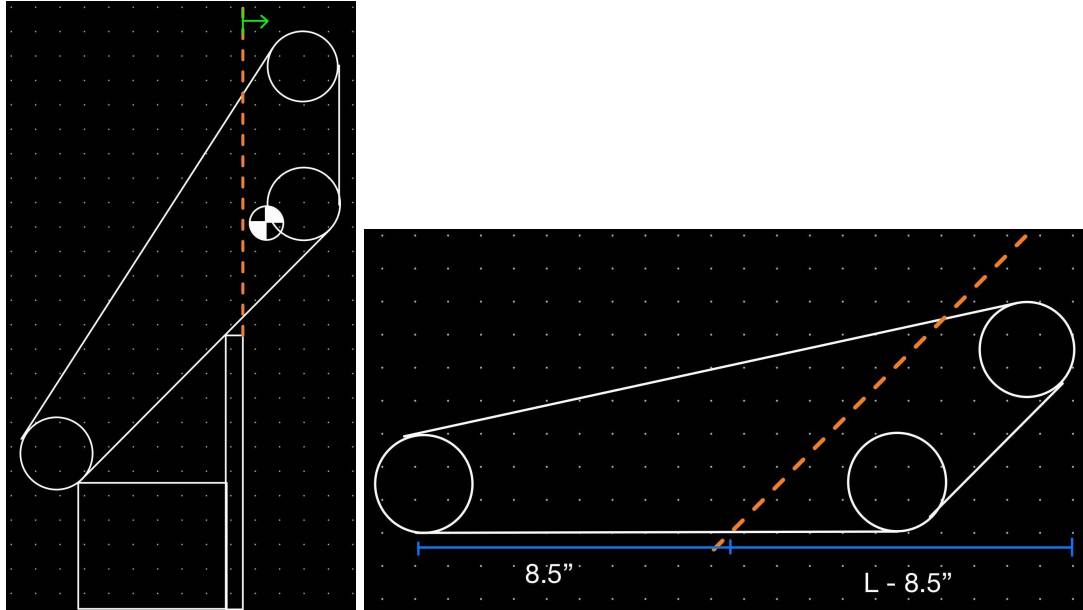


*Figure 5.5.1 (left): Center of mass constraint to tip over the wall while still in contact with step.*

*Figure 5.5.2 (right): Figure 4.5.1 rotated for the robot parallel to the ground.*

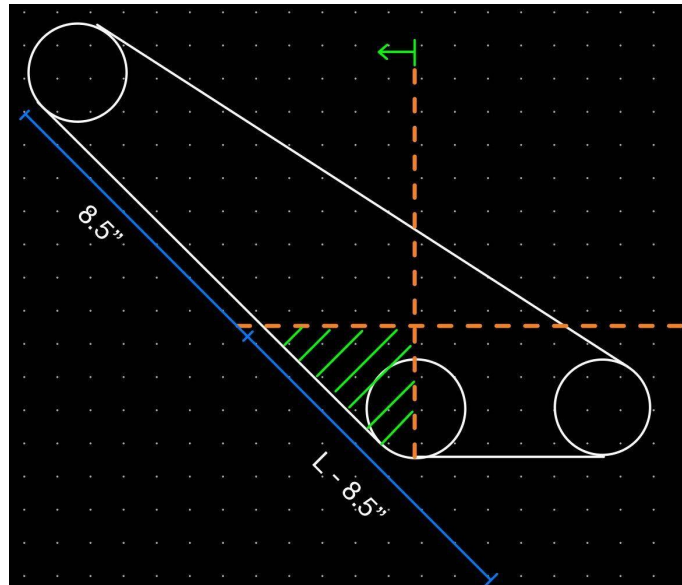


*Figure 5.5.3: SaRR at 45° inclines with both constraints on COM location.*

*Green region meets both constraints. Not to scale.*

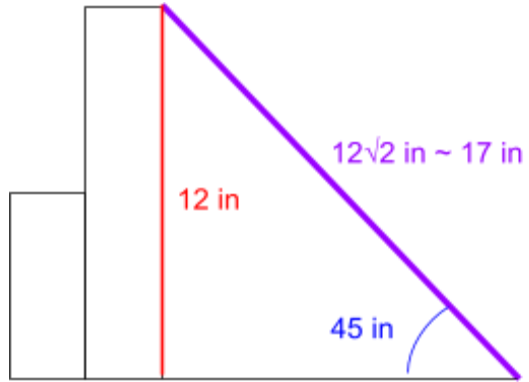


Figure 5.5.4: Triangle to find the front length of the robot such that the max pitch is  $45^\circ$  down the wall.

## 5.6: Load Analysis

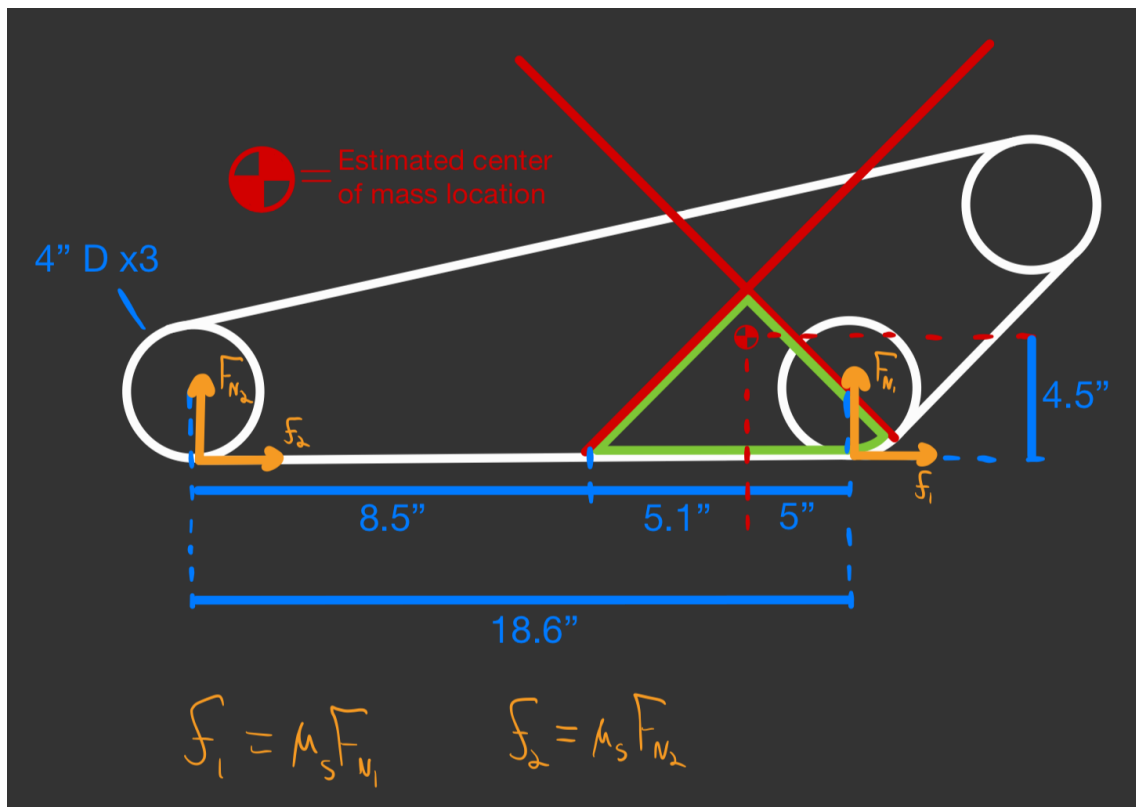


Figure 5.6.1 Load Diagram

Note that the following calculations were done under the initial weight estimate of 60 pounds. However, the same conclusions apply to the final design, as the overall geometry remained the same, thus the new weight simply acts as a rescaling factor. Looking at the full model, a normal force and frictional force are acting on each of the two lower pulleys. By estimating a location for the center of gravity, the loads each pulley wheel experiences can be found. This is accomplished by performing a force and moment balance (hand work featured in images A.6-A.7). The moment was calculated about the center of gravity. When the robot is sitting idle, the forces are as follows:

$$F_{N1} = 43.87 \text{ lbs} \quad F_{N2} = 16.13 \text{ lbs}$$

Since both of these forces are positive, the robot will not tip over. For simplicity, it was assumed that the friction force on each pulley is the maximum static friction force possible without slipping. In reality, this is a greater force than the motor will be able to output, but it is a simple limiting case to analyze. Since the teeth are TPU, the coefficient of static friction is  $\mu_s = 0.8$ . Accounting for this friction force the load forces become:

$$F_{N1} = 32.22 \text{ lbs} \quad F_{N2} = 27.78 \text{ lbs}$$

$$F_x = \mu_s(F_{N1} + F_{N2}) = 48 \text{ lbs}$$

Again, the two normal forces are positive, meaning the treads will begin to slip before the robot tips. With these forces, the total horizontal force pushing the robot forward is found to be 48 lbs. This translates to an acceleration of  $25.76 \text{ ft/s}^2$ , though the actual acceleration is limited by the motor. The SaRR course does not require the robot to drive in reverse beyond turning, but it is still possible to check if the robot can handle it. For this case, consider the full friction forces acting in the reverse direction. This results in the following forces:

$$F_{N1} = 55.48 \quad F_{N2} = 4.52$$

$$F_x = -48 \text{ lbs}$$

This time the normal force on the rear pulley gets rather low, approaching a tipping point. However, this is not a concern since these friction forces are unrealistic and only a test of an extreme limit (full static friction forces in the reverse direction). For the lower frictional forces actually output by the motors, there will be no risk of the robot tipping or slipping.

The final dimensional geometry of the robot was designed using the sketch shown in Figure 5.6.2, which shows the robot on the wall and falling over the wall. This design is close to the minimum length required for a reasonable range of center-of-mass positions, with some extra length for a safety margin.

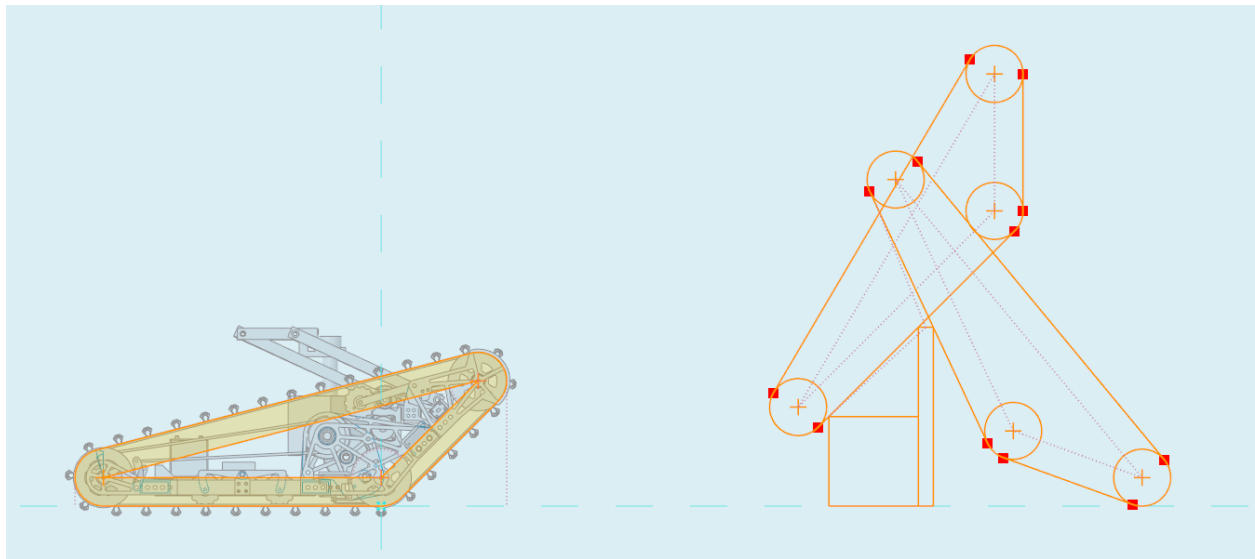


*Figure 5.6.2 Testing Initial Wall-Climbing Geometry*

## 5.7: Design of Medical Kit Placement Mechanism

The mechanism for med-kit placement is a dual parallel four-bar linkage. The two linkages are constrained by a connecting bar and mounted to the front square cross tube built into the robot. A BAG motor from VEX robotics reduced with a 420:1 Versaplanetary gearbox

powers a gear. The gear is coupled with an identical gear attached to a hex shaft. The shaft is constrained to the crank bars of each linkage, powering the entire mechanism. Calculations described in the PDR showed a gear reduction of 60:1 would suffice in lifting the med-kit. However, after initial tests, a gear reduction over 60:1 was necessary due to a greater-than-expected torque requirement to lift the med-kit and to reduce the angular speed of the linkages. To solve this, a 7:1 gear stage was added.

All of the linkage bars are made of 0.75 in by 0.5 in U-channel aluminum stock to provide rigidity to the system. The crank and follower bars were 12 in long and the coupler and ground linkage were 5.375 in long. Measured from the hex shaft, the mechanism can extend the med-kit up to a distance of 16 in and retract it back 5 in. The 5 in retraction of the 1 kg med-kit as well as the placement of the BAG motor below the axis of rotation contributes to the desired location for the robot's center of mass.

A med-kit hook, box, and potentiometer mount were 3D-printed. The hook holds the med-kit by its handle during its placement in the basket. The box is attached to the robot's base acrylic plate to prevent the med-kit from falling out during the wall traversal stage. The potentiometer appended to the output of the med-kit arm was an inexpensive and easy-to-implement analog form of position control. The potentiometer changes resistance as the arm rotates, which is read using an analog-in pin of the Teensy. From there, a control function is run with every single control loop, based upon the error between a reference potentiometer value and the current pot value. The controller implements a proportional-integral control law that keeps the arm at a specified angle with zero steady-state error except for backlash in the arm.

## **5.8: Performance Characteristics**

As discussed in section 3.3, the drivetrain gear ratio of 38:1 results in an output free speed of 29.4 in/s (with 4" diameter wheels). See the spreadsheet linked [here](#) (A.10) for more details on these calculations. Using this value and the course length (~80 ft), a rough run time estimation was 32.5 seconds. The actual run time was significantly longer: roughly 1 minute and 48 seconds. This is mainly because the robot was driven below the maximum free speed to accommodate the autonomous control system. A slower robot has less extreme changes in state, giving the computer time to read sensor values and adjust motor voltages in a gradual, controlled manner. See Section 3.2 for details on energy consumption. Furthermore, because the two treads can turn independently, the robot has a turning radius of zero, allowing for easy maneuverability in the chute.

## **5.9: Mechanical Design Features**

For the drivetrain mechanical design, a tube-and-gusset approach was taken for manufacturability, precision, ease of assembly, and structural integrity. Tube blocks were used to fasten large structural 2" x 1" aluminum box tubes together, and  $\frac{1}{4}$ " lightened aluminum gussets were cut on a CNC water jet for locating key mechanical features. All drivetrain rotating components are doubly supported, and non-cantilevered except for the motor pinion, leading to greater rigidity, increased safety factors on shaft loads, and precise locating with bearings. Figure 5.9.1 shows a side view of the whole robot, featuring dead axles through all pulleys, which have internal bearings installed. These dead axles ensure no torsional load on the shafts through the drive pulleys.

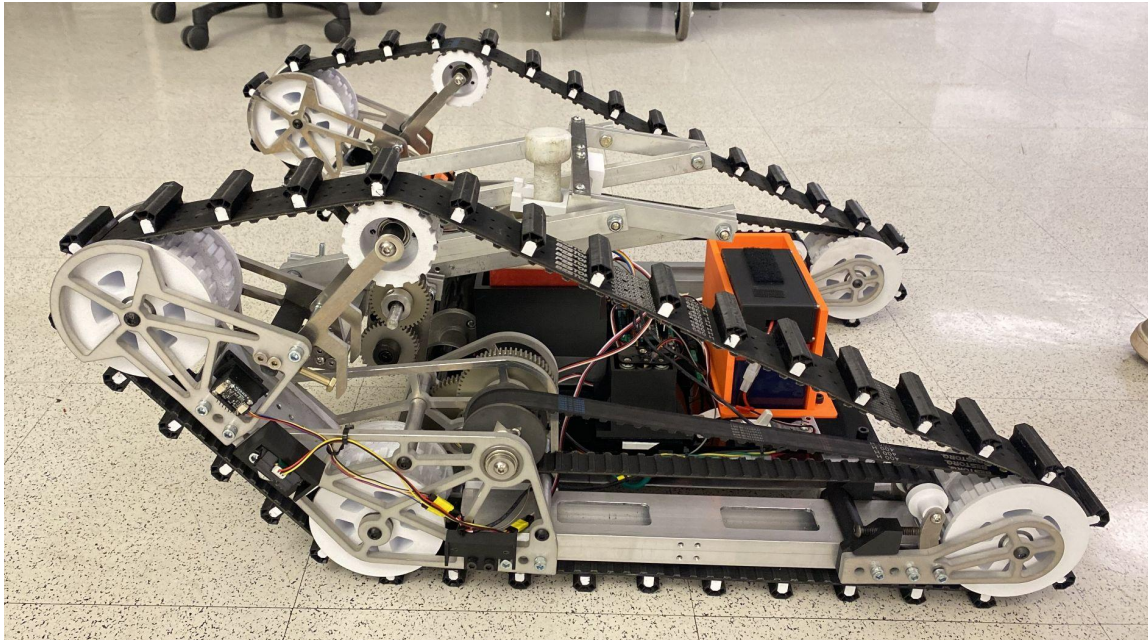


*Figure 5.9.1 Side Profile*

The rear pulley was chosen as the primary drive pulley due to it having the most teeth engagement with the primary drive belt, minimizing the chance of tooth slippage. Furthermore, the gearbox and motors were located forward and low, for an ideal CG as computed previously. These gearboxes tightly package a two-stage gear reduction and transmit power across the entire length of the robot in another belt reduction. An interesting design feature is that this internal belt was packaged on the same vertical plane as the main drive belt, keeping space in the center of the robot clear and keeping the drivetrain extremely space-efficient while also providing a nice design challenge. This internal belt powers the rear drive pulley using a special 3D-printed “pulley within a pulley” design, where the drive pulley has a small diameter pulley profile sandwiched by a large diameter pulley profile. This allows the thin internal belt to engage with these center teeth on the small diameter section, while the thick main drive belt engages only with the large diameter section, such that one belt is packaged on top of the other, as shown on

the right of Figure 5.9.1. Additionally, the gearbox shafts are all supported with two bearings despite there being three parallel plates, such that misalignment issues are mitigated.

As a belt-driven system, the drivetrain requires tensioners, which were designed as lever systems. For the internal drive belt, lever tensioners were built using bearings that ride along the outside of the belt, providing smooth, continuous tension. Bolts are tightened to apply more force to the lever, pushing on the belt for more tension. For the outer main drive belt, a large lever system was devised with a dead-axle idler pulley applying tension to the belt. This system also uses bolts that can be tightened or loosened to adjust the tension on the main drive belt. After falling over the wall repeatedly, the drivetrain gussets settled into new positions since the bolt holes were all clearance fits, so more tension was applied subsequently.

The med-kit placement arm originally was driven by a belt, which was found to be prone to slippage due to a small-pitch tooth profile. The mechanism was switched to a gear system, and the issue was resolved. The med-kit placement linkages also feature bushings through each joint, ensuring smooth and low-backlash operation.

The drivetrain was originally designed to support two idler pulleys per side to distribute the load of the robot on a rocker system that would conform to the terrain. However, this was deemed unnecessary after testing without rockers. Another drivetrain feature is the design of the front gussets, which protrude just below the teeth of the main belt to take the impact of shocks from falling off of the wall. This is important to protect the pulleys from shock loads.

Another critical design feature is the prevention of boring out 3D-printed pulley bores. While prototyping, it was found that printed plastic pulleys were easily bored out by a hexagonal shaft, so aluminum inserts were cut on the water jet to transfer the load to the pulleys without boring them. In Figure 5.9.1, an example of these aluminum inserts is seen in the gray

3D-printed nylon pulley in the gearbox, which features a hexagonal hole that transmits torque from the hex shaft. The gearboxes of the drivetrain and med-kit arm are the only instances of live-axle torque transmission throughout the robot.

The gearbox assembly can be seen in a side profile, with two gear reductions and one belt reduction in Figure 5.6.2. Three gearbox plates with three standoffs each retain a parallel relationship between the plates. The gearbox position contributes to the desired center of mass as previously described. The gearbox is shown in more detail, with the transmission belt visible in Figure 5.6.3. The bend in the belt is due to a bearing tensioner tightened by turning bolts, making it a very secure tensioning system. Figure 5.9.4 demonstrates the pulleys used in the drivetrain. The pulleys show the low-diameter center and large-diameter side teeth. The transmission belt engages with the narrow center, and the lower diameter in the center also allows the bolt heads of the teeth to pass through the pulley without contacting. This design worked well and also eliminated the need for live axles, meaning that there was no risk of boring out center holes or putting torsional loads on shafts. Bearings are pressed nicely into the pulleys and sit flush with each side.

Furthermore, testing revealed that the shock induced while descending the wall reset the Teensy, causing the program to temporarily pause. To mediate this issue, a shock absorption system was developed using an elastic TPU base that acts as a damped spring upon impact. The Teensy was mounted to this base, and further testing demonstrated that this solution had successfully resolved the resetting issue.

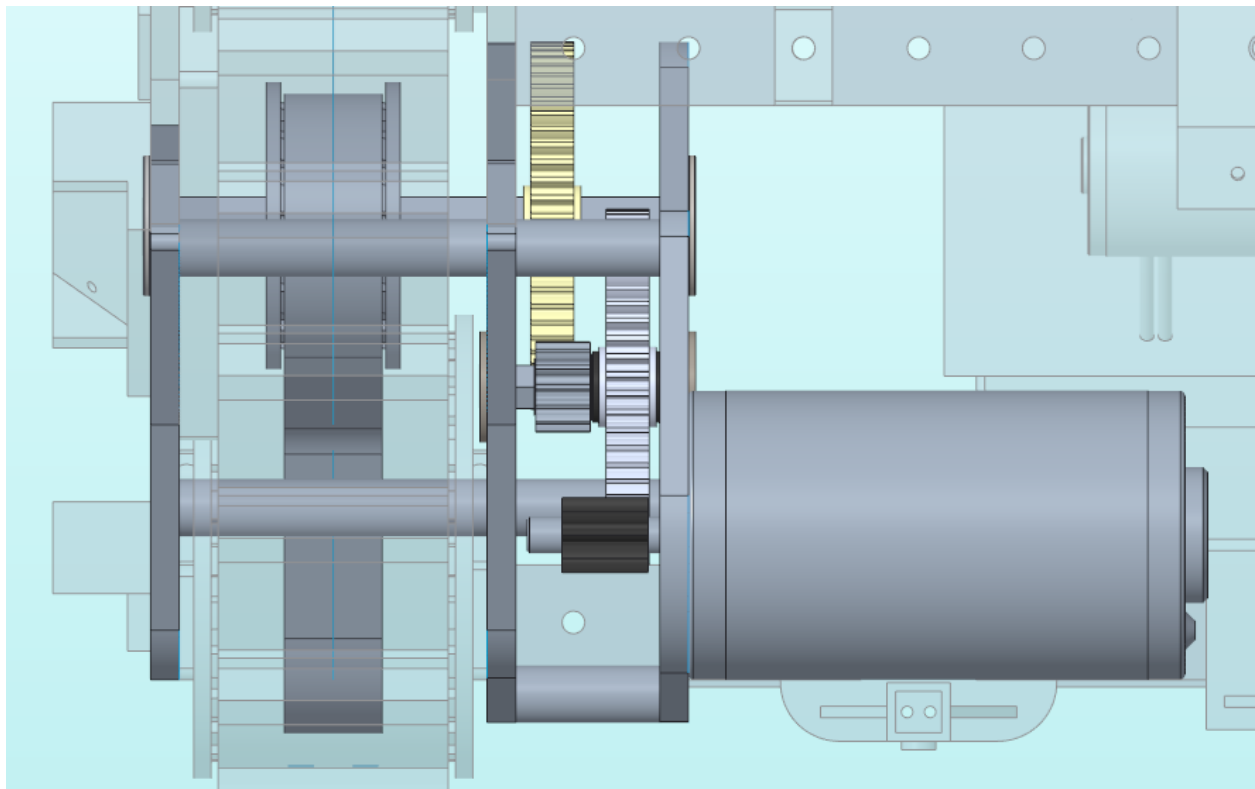


Figure 5.9.2 Gearbox Front Profile

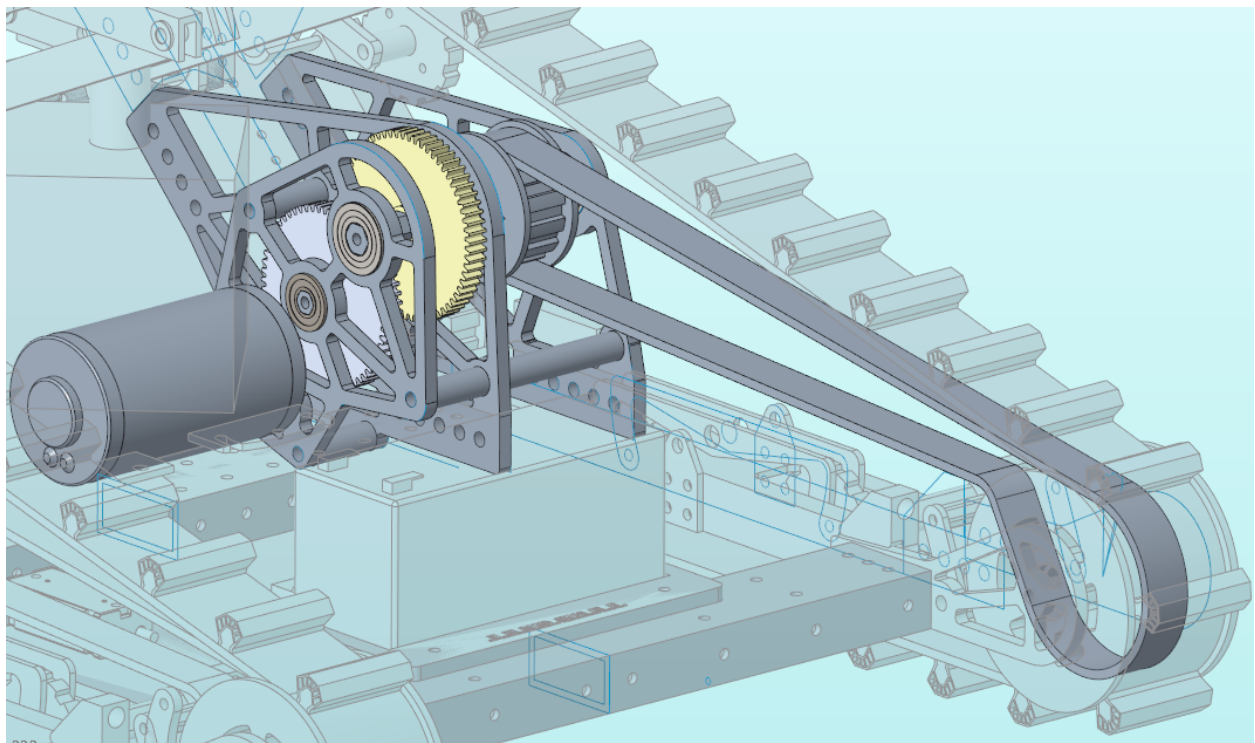
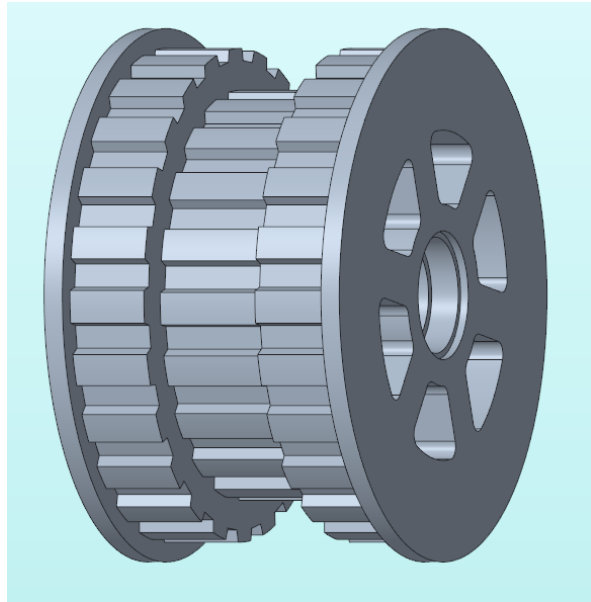


Figure 5.9.3 Gearbox and internal transmission belt, surrounded by the outer main drive belt



*Figure 5.9.4 Specialized pulley*

## **5.10: Control System**

The robot was designed to operate autonomously using eight attached sensors and the previously-mentioned potentiometer for the med-kit arm. Three of these are cadmium sulfate sensors provided by the machine shop, used for finding light sources emitted by the ramp and basket (goal) along the course. The remaining five are used for distance sensing; three are SHARP infrared (IR) distance sensors provided by the machine shop, and the other two are Time of Flight (ToF) distance sensors purchased from Adafruit.

A diagram of the electronics, including the batteries, Teensy controller, and sensors, is provided below in Figure 5.10. Note that this diagram does not include the motors, but does include the pulleys and a simplified version of the chassis for orientation. Additionally, note that this diagram is not to scale.

Two ultrasonic distance sensors, purchased from Adafruit with the ToF sensors, were ultimately not used. The team was satisfied with the strong performance of the ToF sensors,

which were rated to have a range of 1 to 1300 mm. The ultrasonic sensors acted as a backup in case of an issue with the other sensors. The team was aware that these would potentially have had worse performance due to the wide angles at which the sonic waves could be emitted (compared to the narrow beams of the ToF sensors). These were luckily very cheap, at only \$4 apiece.

The program for autonomous navigation was written in stages corresponding to the current obstacle being traversed. This method of breaking up the course into various steps allowed for simplicity in the control, and made it such that only the necessary sensors for each obstacle were actively being read; however, because this requires the obstacles to appear in the assigned order (ramp, chute, wall), it is not as generalizable to all situations.

The program stages are described below:

- 1) Ramp Approach - All three CdS sensors are in use. The robot uses a modified version of the originally provided light-finding algorithm, in which the turn amount is proportional to the “error” or difference in readings between the left and right sensors. The robot uses the light to get onto the ramp; once the light reading for the center sensor is strong enough, the transition to the next stage is activated.
- 2) Ramp Traverse - The two SHARP sensors on the side, as well as the ToF sensors, are in use. The robot looks for large jumps in the values being read from the SHARP sensors, as these indicate that the sensors are no longer looking at the ramp; it then centers itself accordingly. Once valid values are read from the ToF sensors, indicating that the chute walls are present, the program transitions to the next stage immediately.

- 3) Chute Traverse - The two ToF sensors and the front SHARP sensor are in use. With the turn amount once again proportional to the difference between the two sensors, the robot centers itself along the chute until it reaches a specified distance from the wall, at which it transitions immediately to the next stage.
- 4) Wall Traverse - The robot simply drives forward for 12 seconds. The team found, in testing, that the robot was able to consistently center itself during this step without relying on any sensors.
- 5) Light Finding - The left and right CdS sensors are in use, along with the front SHARP sensor. Using a similar algorithm to the first stage, the robot navigates toward the basket light until it is a specified distance away from it. The robot then extends the med-kit arm out, releasing the med-kit into the basket, before stopping and reversing.

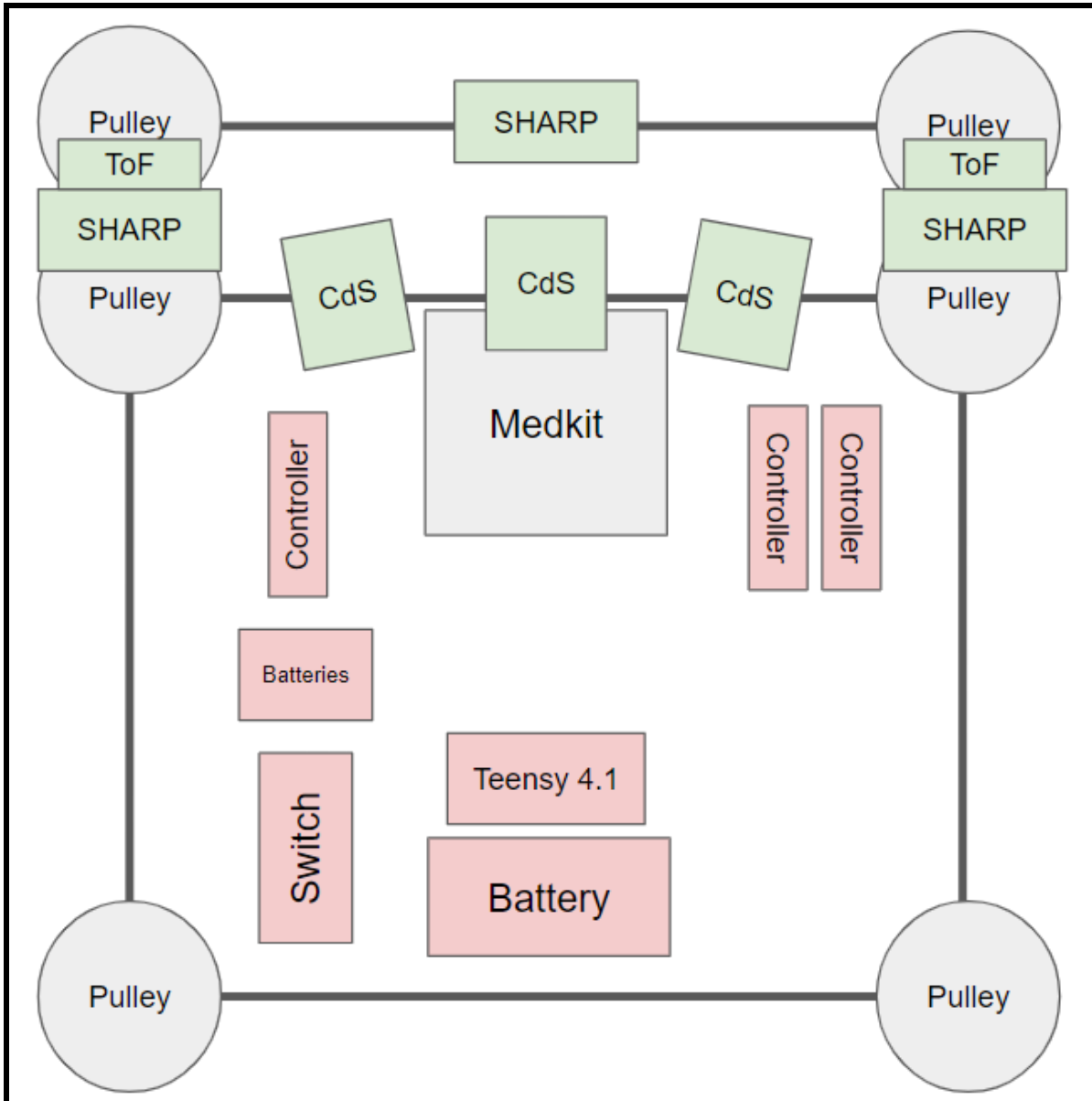
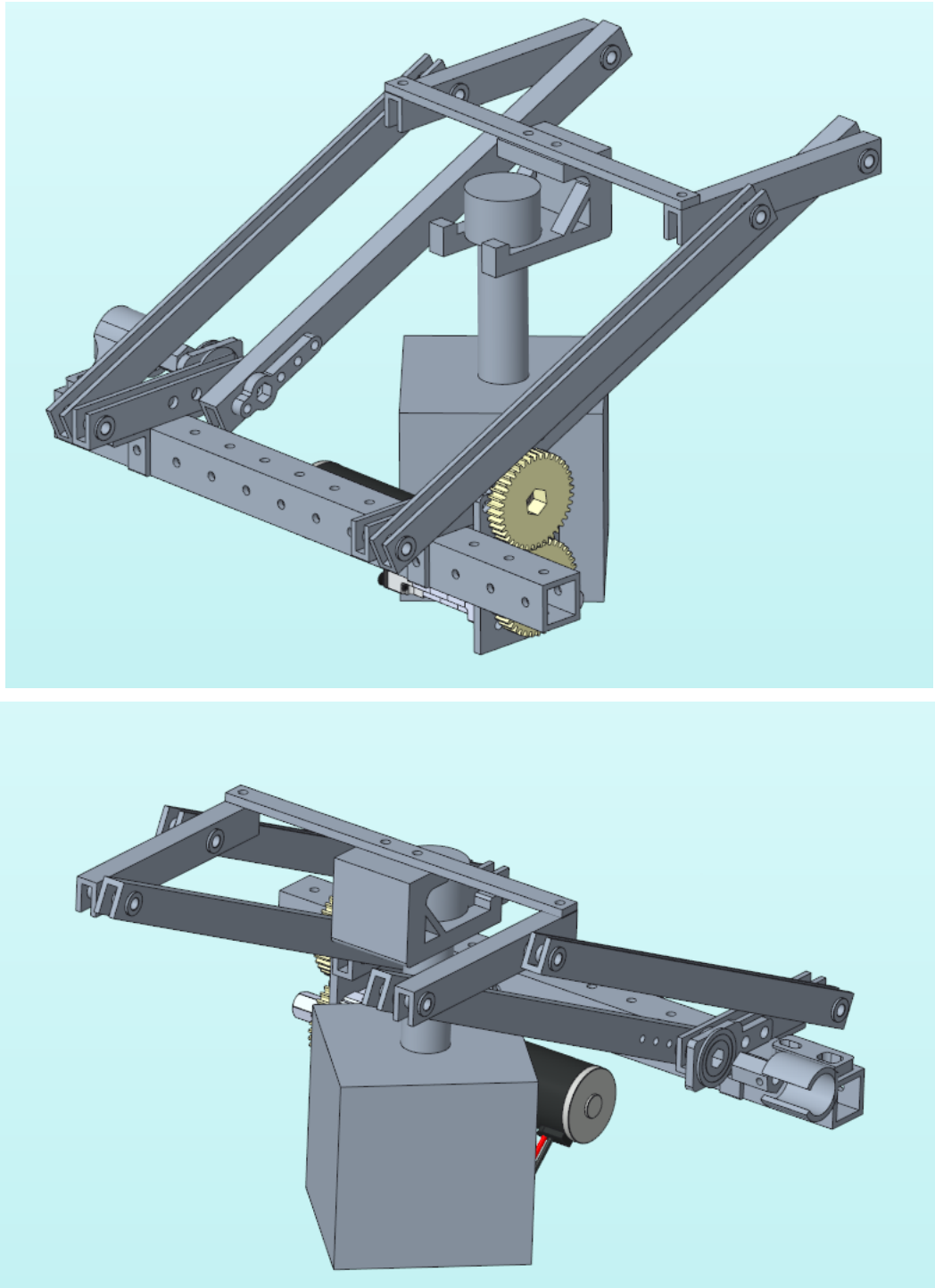


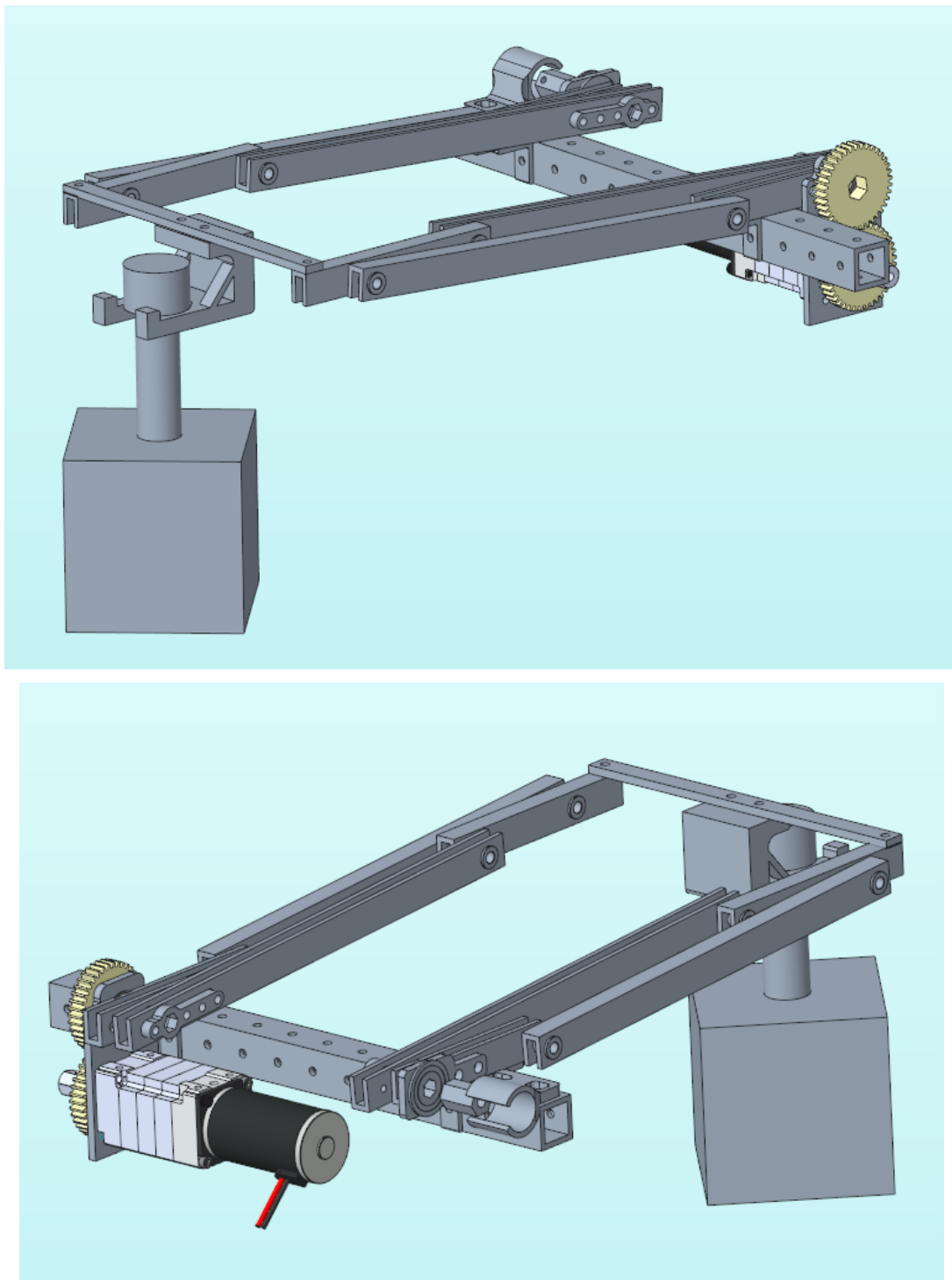
Figure 5.10 - Configuration of Robot Electronics and Sensors (Not to Scale)

A significant portion of the program was dedicated to debugging these stages and ensuring the proper functionality of the robot. For the full program in use, see Appendix A.9.

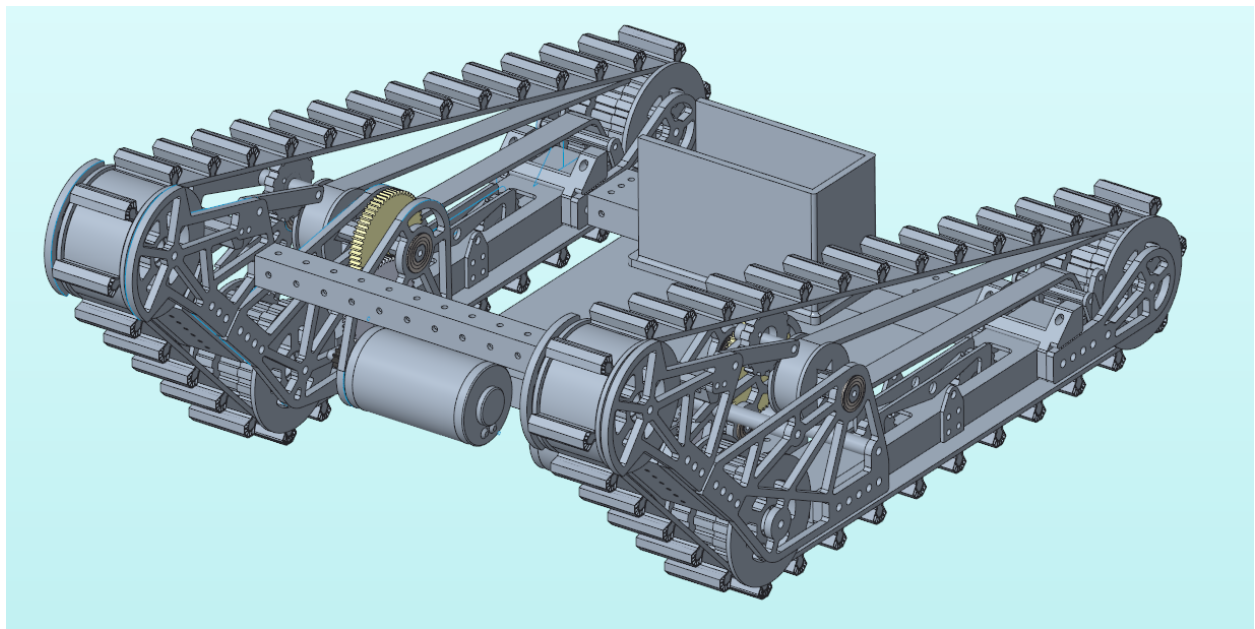
## ***6. CAD Profiles and Engineering Drawings***

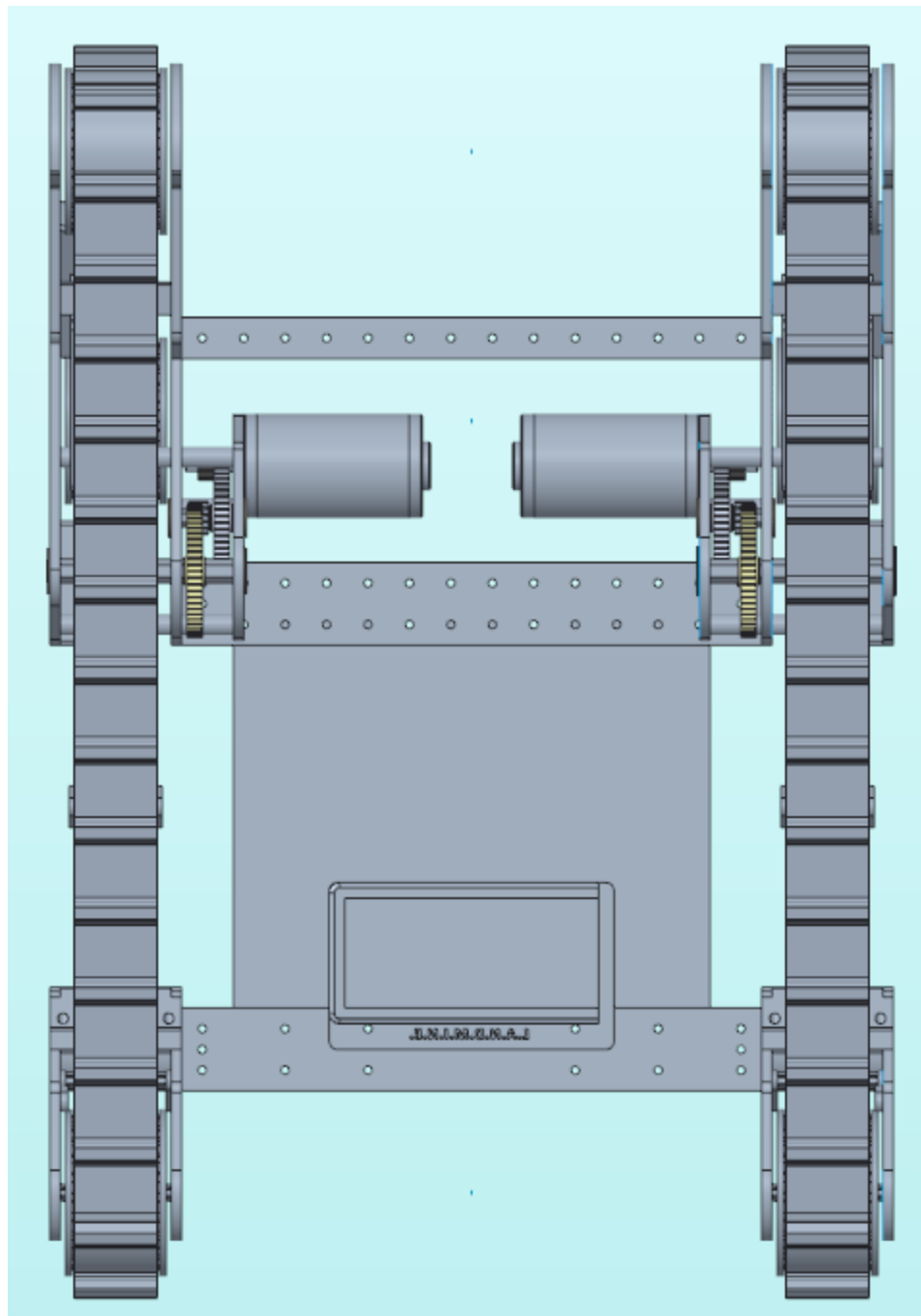


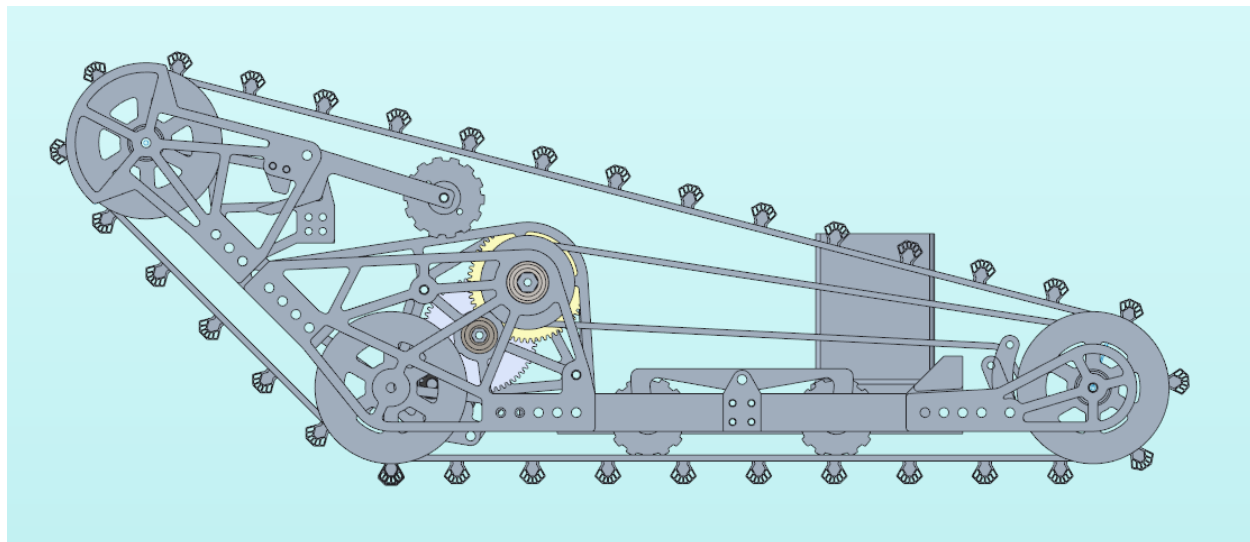
*Figures 6.1.1 and 6.1.2: Full Med-Kit Delivery Assembly Retracted Position,  
Front and Rear Perspectives*



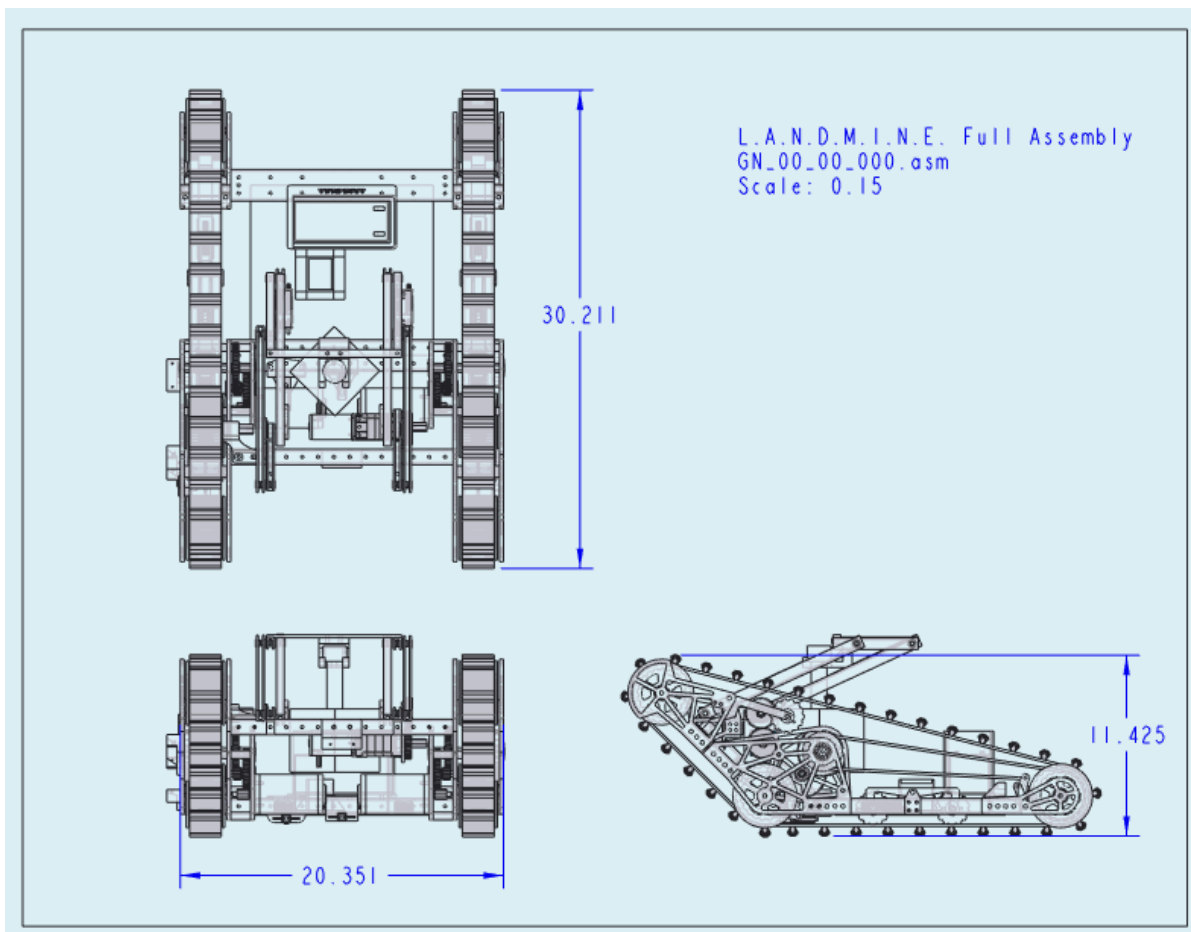
*Figures 6.1.3 and 6.1.4: Full Med-Kit Delivery Assembly Extended Position, Front and Rear Perspectives*

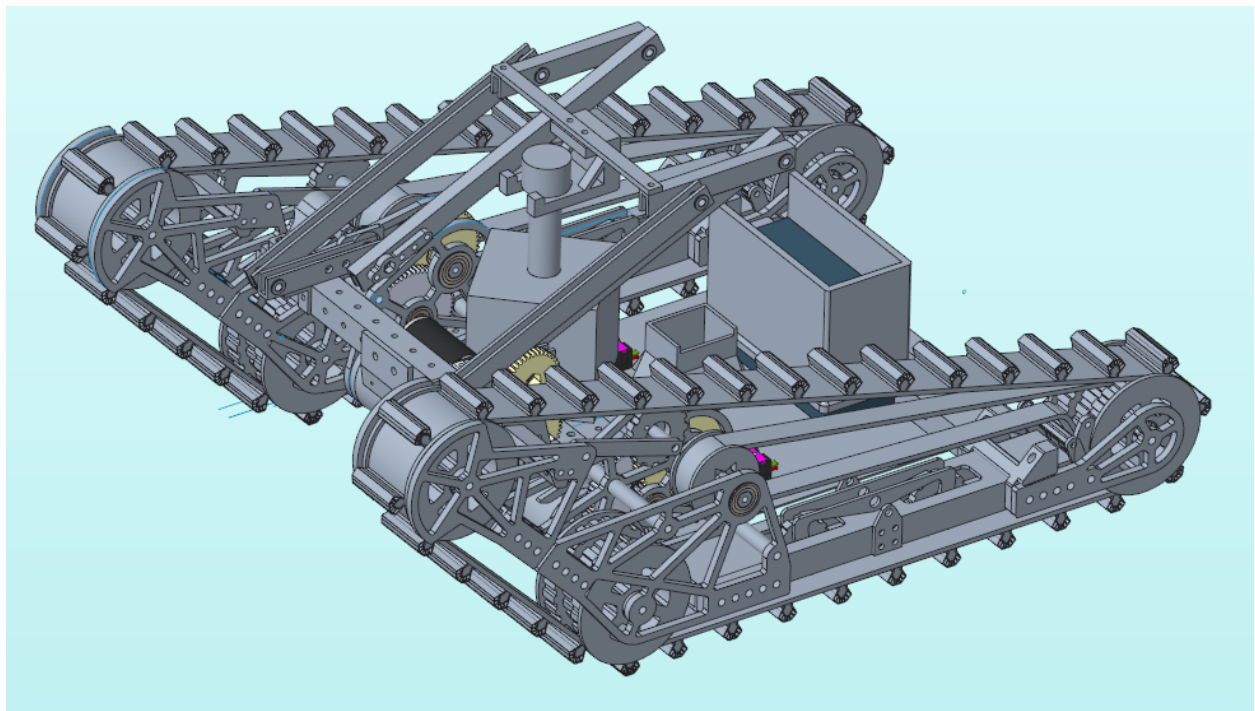






Figures 6.2.1, 6.2.2, and 6.2.3: Drivetrain Isometric, Top, and Side View





*Figures 6.3.1 and 6.3.2: Master CAD Views*

## **7. Test Results**

The robot was able to complete the full course autonomously three times in practice before the demonstration session. The data for this section was taken from the second of these three runs, which was recorded. This video is provided in Appendix A.8.

This run-through of the course took approximately 1 minute and 48 seconds. Rough estimates for the distances were calculated by treating each square tile on the floor as a 1-square-foot area. Breaking this down section by section:

- The robot began the course facing 90 degrees away from the ramp light and from approximately 7 feet away. Finding the light and driving onto the ramp took 18 seconds. For speed calculations, this equated to about 4 seconds for a 90-degree point turn, and a forward travel speed of 0.5 feet per second.
- The robot entered the chute after about another 18 seconds.
- The robot made contact with the wall about 1 minute into the run; thus, it took 24 seconds to navigate through the chute.
- The robot was fully over the wall 10 seconds later.
- The robot spent the remaining 38 seconds navigating toward the basket, placed around 20 feet away. This equates to an average speed of slightly less than 0.5 feet per second.

The med-kit delivery mechanism took roughly 0.6 seconds to rotate approximately 160 degrees, meaning that the med-kit arm mechanism rotates at roughly 81 rpm. A slower placement of the med-kit would likely ensure fewer failures, but the current speed has proven adequate for the robot's goals.

Extensive testing revealed that running the robot faster for the light-finding sections caused large amounts of instability in driving, as it would oscillate greatly between turning right and left instead of following a relatively straight path. Similar findings arose when attempting to run it faster through the chute. The robot would slip on the ramp and wall when pushed faster, which, especially in the case of the wall, would have only increased the time of course completion or chances of failure. Thus, except for the 1-3 seconds for pauses upon transitioning to ramp traversal or depositing the med-kit, this is believed to be the fastest that the robot can reliably and smoothly run through the course.

During the final presentation, the company's predicted performance time was around the middle of the pack relative to the other four teams present. Unfortunately, several issues came up that complicated the completion of the course during the demonstration. Most notably, the Teensy board gave out during the first attempt at wall traversal; the left SHARP sensor required replacement as it began giving faulty values; and the med-kit arm hook snapped while depositing the med-kit. However, the robot was able to complete the course in full on the sixth attempt, taking roughly the expected amount of time. Overall, these are very promising results and indicate that this design can likely be developed into a deployable SaRR for real-world applications, after appropriate modifications to promote robustness.

## ***8. Conclusions and Further Work***

Overall, the SaRR was able to perform all aspects of the mission in a robust package. It is a product that may be deployable with additional refinement. The first area of focus is the med-kit delivery system. The biggest concern with the current product is the packaging of the med-kit and its reaction to large shocks, such as those experienced while going over the wall. Additionally, encoders on the motor itself would prove beneficial to reading arm position. Furthermore, an additional area of focus may be put into the robustness of the drive-train by replacing the PLA items with high-strength materials. Work may be put into the sensor mounts to shield them from any potential damage. Similarly, the wiring harness can be improved to shield critical components such as the Teensy. The tensioners and belt may also be improved to reduce the stretching and increase lifespan. Lastly, a more generalized code should be developed for the case that the robot is deployed in an unknown environment, with an array or order of obstacles that differs from the test course. Obstacle identification can be a helpful feature for such environments, allowing the robot to select a run method that would be optimal for traversing the specific obstacle ahead.

As mentioned earlier, during the final demonstration, a few issues came up while demoing. The main source of issues during the presentation was the unreliability of the IR sensors that our SaRR used to navigate the ramp; the sensors output poor, inconsistent data which reduced the effectiveness of the feedback control. Additionally, the Teensy burnt out mid-demo and needed to be replaced. To alleviate these issues, the company would prefer to source better sensors and, if the infrastructure is available, look into custom PCBs. More specifically, it would be helpful to replace all of the SHARP sensors with Time of Flight sensors, since they functioned well and reliably for the chute traversal portion.

## **9. References**

- [1] "Four-Legged 9/11 Heroes." *Four-Legged 9/11 Heroes | National September 11 Memorial & Museum*, 911memorial.org, www.911memorial.org/connect/blog/four-legged-911-heroes. Accessed 1 Nov. 2024.
- [2] Bovsun, Mara. "The Lasting Impact of the Dog Heroes of 9/11." *American Kennel Club*, American Kennel Club, 9 Sept. 2024, www.akc.org/expert-advice/family-dog/the-legacy-of-9-11-dogs/.
- [3] Brading, Thomas. "20 Years Later: Search and Rescue Soldiers Reflect on 9/11." *Www.Army.Mil*, U.S.Army, 8 Sept. 2021, www.army.mil/article/249870/20\_years\_later\_search\_and\_rescue\_soldiers\_reflect\_on\_911.
- [4] "Illness and Advocacy after 9/11." *Illness and Advocacy After 9/11 | National September 11 Memorial & Museum*, 911 Memorial & Museum, 911memorial.org/illness-and-advocacy-after-911. Accessed 1 Nov. 2024.
- [5] "Toxins and Health Impacts: Health Effects of 9/11 - WTC Health Program." *Centers for Disease Control and Prevention*, Centers for Disease Control and Prevention, 23 Oct. 2023, www.cdc.gov/wtc/exhibition/toxins-and-health-impacts.html.
- [6] "Stair Climbing Robot." YouTube, uploaded by themachinelabinc.8952, Sept. 2023, <https://www.youtube.com/watch?v=b5KlahGb5P8>.
- [7] Nosenchuck, Daniel. "Introduction to Mechanisms: Linkages and Applications." MAE 322, Fall 2024, Princeton University Department of Mechanical and Aerospace Engineering, Princeton, NJ. Lecture.

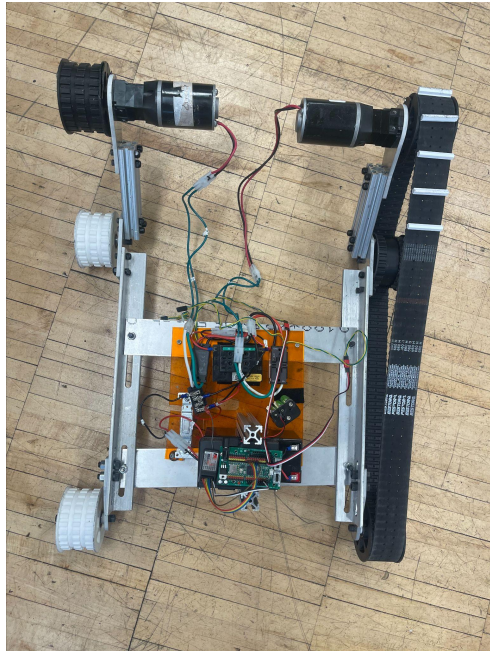
[8] Walters, Joanna. “9/11 Health Crisis: Death Toll from Illness Nears Number Killed on Day of Attacks.” *The Guardian*, Guardian News and Media, 11 Sept. 2016, [www.theguardian.com/us-news/2016/sep/11/9-11-illnesses-death-toll](http://www.theguardian.com/us-news/2016/sep/11/9-11-illnesses-death-toll).

[9] “Cim Motor - VEXPRO Motors - VEX Robotics.” *VEX Robotics Motor Data - CIM Motor (217-2000)*, Vex Robotics, [motors.vex.com/vexpro-motors/cim-motor](http://motors.vex.com/vexpro-motors/cim-motor). Accessed 1 Nov. 2024.

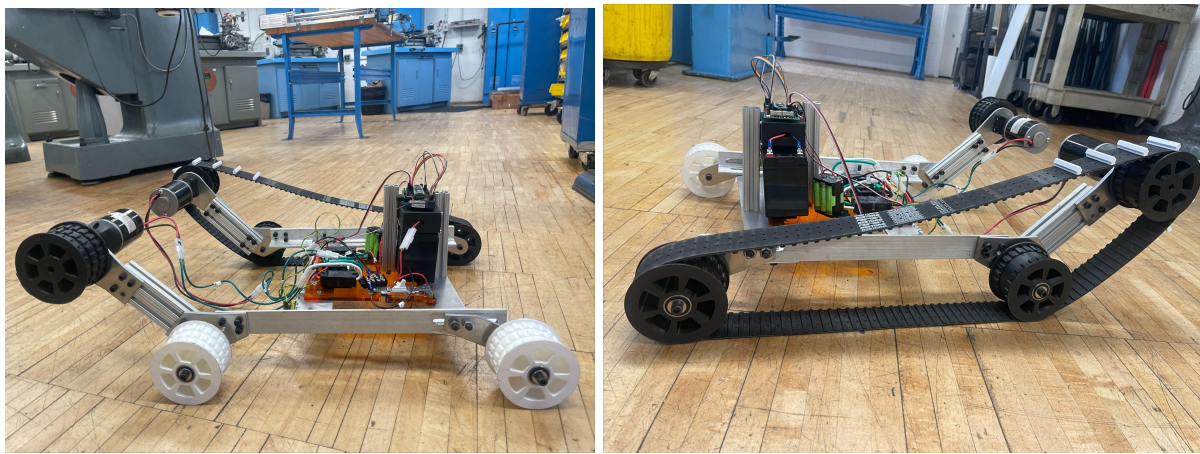
[10] stm32duino. “Stm32duino/VL53L4CD: Arduino Library to Support the VL53L4CD Time-of-Flight High Accuracy Proximity Sensor.” *GitHub*, [github.com/stm32duino/VL53L4CD](https://github.com/stm32duino/VL53L4CD). Accessed 12 Dec. 2024.

## A. Appendix A

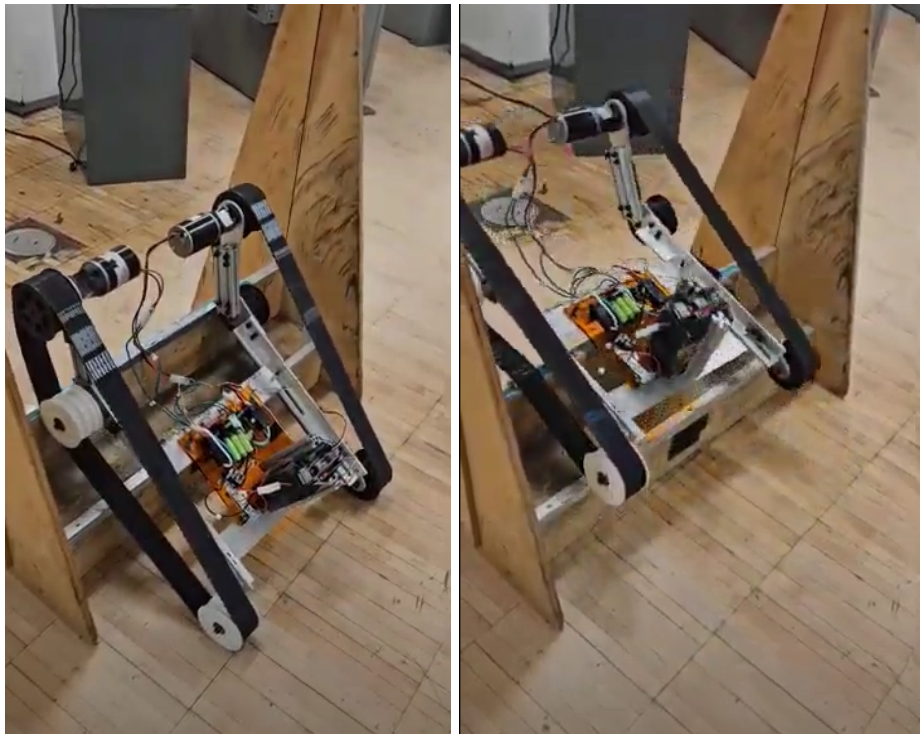
### Prototype Photos



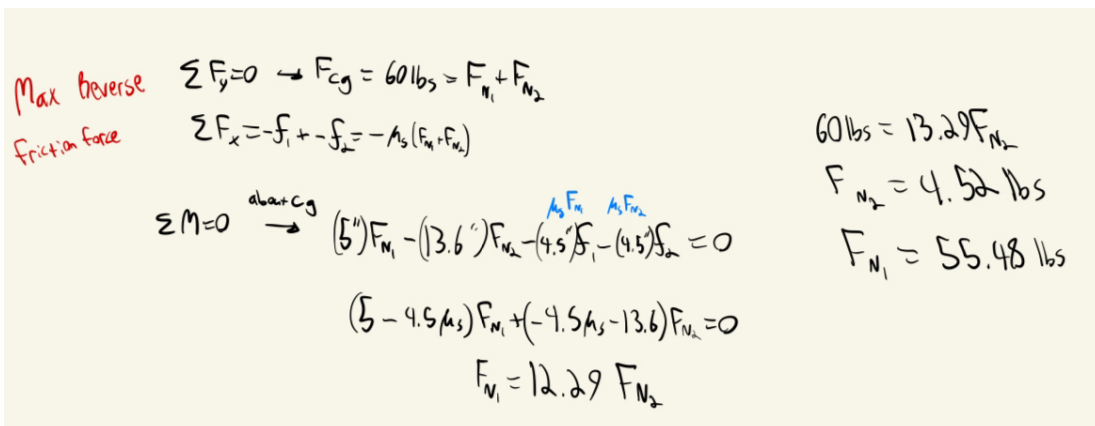
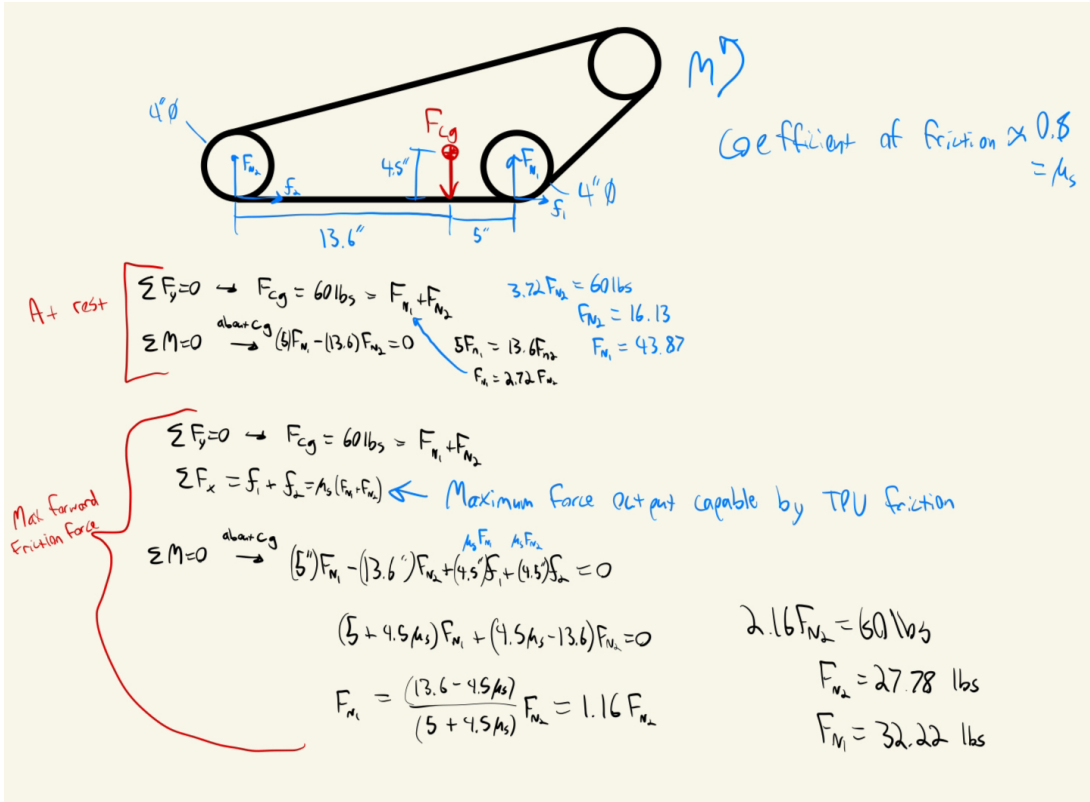
A.1: Top view of the prototype.



A.2 and A.3: Side views of the prototype, with only one tread attached for a clear view of the pulleys and chassis.



*A.4 and A.5: Photo of the prototype during the wall climb and just before clearing.*



#### A.6 and A.7: Load Calculations

[https://drive.google.com/file/d/1BY243\\_PszTx9jJaLbw3LFu3cDQunQJpD/view?usp=sharing](https://drive.google.com/file/d/1BY243_PszTx9jJaLbw3LFu3cDQunQJpD/view?usp=sharing)

A.8: Full Course Completion Video

[https://docs.google.com/document/d/1HMRfCSE\\_O0ndxN4lydKOYG1PoHX2yyWUtcsnTx8UhPs](https://docs.google.com/document/d/1HMRfCSE_O0ndxN4lydKOYG1PoHX2yyWUtcsnTx8UhPs/edit?usp=sharing)

[/edit?usp=sharing](#)

*A.9: Final Autonomous Navigation Code*

[https://docs.google.com/spreadsheets/d/1LmkrXZtFW-KpDTjuTs3ogg7KpqVGk\\_mAJu1k9m3PMk4](https://docs.google.com/spreadsheets/d/1LmkrXZtFW-KpDTjuTs3ogg7KpqVGk_mAJu1k9m3PMk4/edit?gid=615911138#gid=615911138)

[/edit?gid=615911138#gid=615911138](#)

*A.10: Motor Design and Gearing Calculator*

[https://docs.google.com/spreadsheets/d/11PfsShCGJi34b7P-eAjonLIRMNFzT96l-Nu6ZPmWnLk](https://docs.google.com/spreadsheets/d/11PfsShCGJi34b7P-eAjonLIRMNFzT96l-Nu6ZPmWnLk/edit?gid=0#gid=0)

[/edit?gid=0#gid=0](#)

*A.11: Drivetrain Force/Torque Calculator*